

Automatic Phase Identification of Earthquake Based on the UBDN Deep Network

Jianxian Cai

Institute of Disaster Prevention

Xun Dai

Institute of Disaster Prevention

Gao zhitao (✉ gzt@cidp.edu.cn)

Institute of Disaster Prevention <https://orcid.org/0000-0002-7667-3370>

Yan Shi

Institute of Disaster Prevention

Full paper

Keywords: U-net, Bidirectional Long Short Term Memory, Phase identification, Wenchuan aftershocks

Posted Date: April 29th, 2021

DOI: <https://doi.org/10.21203/rs.3.rs-417923/v1>

License: © ⓘ This work is licensed under a Creative Commons Attribution 4.0 International License.

[Read Full License](#)

Version of Record: A version of this preprint was published at Journal of Intelligent & Fuzzy Systems on December 3rd, 2021. See the published version at <https://doi.org/10.3233/JIFS-211792>.

1 **Automatic phase identification of earthquake based on the**
2 **UBDN deep network**

3 Author #1: Jianxian Cai, Institute of Disaster Prevention, jianxian.cai@hotmail.com

4 Author #2: Xun Dai, Institute of Disaster Prevention, daixun0615@qq.com

5 Corresponding Author #3: Zhitao Gao, Institute of Disaster Prevention,
6 e228319@163.com

7 Author #4: Yan Shi, Institute of Disaster Prevention, windsor33@163.com

8

9

10

11

12

13

14

15

16

17

18

19

20

21

22 **Abstract**

23 Seismic data obtained from seismic stations are the major source of the information
24 used to forecast earthquakes. With the growth in the number of seismic stations, the
25 size of the dataset has also increased. Traditionally, STA/LTA and AIC method have
26 been applied to process seismic data. However, the enormous size of the dataset reduces
27 accuracy and increases the rate of missed detection of the P and S wave phase when
28 using these traditional methods. To tackle these issues, we introduce the novel U-net-
29 Bidirectional Long-Term Memory Deep Network (UBDN) which can automatically
30 and accurately identify the P and S wave phases from seismic data. The U-net based
31 UBDN strongly maintains the U-net's high accuracy in edge detection for extracting
32 seismic phase features. Meanwhile, it also reduces the missed detection rate by applying
33 the Bidirectional Long Short-Term Memory (Bi-LSTM) mode that processes timing
34 signals to establish the relationship between seismic phase features. Experimental
35 results using the Stanford University seismic dataset and data from the 2008 Wenchuan
36 earthquake aftershock confirm that the proposed UBDN method is very accurate and
37 has a lower rate of missed phase detection, outperforming solutions that adapt
38 traditional methods by an order of magnitude in terms of error percentage.

39 **Keywords**

40 U-net; Bidirectional Long Short Term Memory; Phase identification; Wenchuan
41 aftershocks

1 Introduction

Seismic phase identification is a solid foundation for earthquake prevention and disaster reduction work (e.g., earthquake early warning systems). Previously, manual identification and travel timetable-based calculations were the two main methods used to analyze various seismic phase data and identify seismic phases. In recent years, with the growth in the number of seismic stations, the amount of seismic data available has also increased significantly. The efficiency and accuracy of manual identification has therefore gradually decreased. At the same time, the noise pollution caused by urbanization leads to higher rates of missed detection of low-level earthquakes. Manual identification can no longer maintain the accuracy and efficiency of phase detection. Seismic phase automatic identification is thus becoming a more widely used approach (Wu et al. 2004). It improves efficiency and reduces cost through faster processing of seismic data and higher identification rates.

Nowadays, seismic phase automatic detection is widely used to detect earthquakes. It utilizes characteristic equations, taking into account different parameters (e.g., amplitude and frequency). Thresholds are set based on these equations. Once a detected seismic phase reaches a preset threshold, the occurrence of an earthquake can be confirmed and its arrival time determined. Several methods are applied to seismic phase automatic identification. The Short-/Long-Term Average (STA/LTA) method uses the relationship between the average ratio of the short and the long time windows (Allen et al. 1978; Baer et al. 1987; Withers et al. 1998), and the threshold value. The Akaike

information criterion (AIC) method is used to find the best division point (Akaike et al. 1974; Sleeman et al. 1998; Akazawa et al. 2004; Liu et al. 2013), and the fractal dimension method then uses the fractal dimension value to determine the first arrival point (Boschetti et al. 1996; Chang et al. 2002; Han et al. 2002; Cao et al. 2004; Tang et al. 2017). These methods are affected by environmental noise and have poor stability, resulting in low accuracy of identification and high rates of missed detection. In addition, the recognition results of these methods are significantly affected by the selection of features, functions, and parameters. The results often differ greatly from expectation when the signal-to-noise ratio (SNR) is low. Therefore, these methods are not efficient in seismic phase automatic identification when dealing with very large datasets.

Artificial intelligence and big data are now the most effective methods used to manage massive datasets (Dai et al. 1997). Artificial neural networks have been developed and widely applied to the automatic identification of seismic phases because of their strong learning ability. The size of the dataset caused by the increasing number of seismic stations can therefore be addressed by applying neural networks. When handling massive datasets, an artificial neural network requires both training and converging data and the determination of related parameters (e.g., neurons; layers) through continuous experiment (Zhang et al. 1998; Wang et al. 2006; Wang et al. 2008). To some extent, the application of neural networks to the automatic identification of seismic phases is limited due to the training processes required.

84 To address these limitations, a deep learning method has been developed for
85 solving the neural network's training difficulties (Ross et al. 2018). In particular, the
86 Convolutional Neural Network (CNN) approach to deep learning has been widely used
87 in recent years. The CNN is classified according to multi-, shallow, and deep layers of
88 convolutional structures. The multilayer convolution structure learns the features of the
89 different levels, while the shallow layer learns the local features of the signal.
90 Meanwhile, the deep convolutional layer is better at learning abstract features, which
91 improves the classification and generalization capabilities of the CNN model compared
92 to others. The deep convolutional layer structure of CNN is widely used in seismic
93 signal noise reduction, seismic phase classification, and related matters (Zhao et al.
94 2019). Perol applied CNN to seismic phase identification (Perol et al. 2018), designing
95 an eight-layer CNN with high identification accuracy. Ross manually annotated the
96 dataset and used CNN for training (Ross et al. 2018). Experimental results have shown
97 that this trained CNN model has high identification accuracy. Meanwhile, the
98 identification effect with low SNR and different regions is still within the ideal range.
99 Yu Ziyi input three-component seismic data into a 17-layer Inception model based on
100 CNN after high-pass filtering (Yu Ziyi et al. 2018). At the same time, 100 datasets with
101 different degrees of noise were added and tested. Their results proved that the deep
102 learning method has a high tolerance for noise and is more stable than the AR-
103 AIC+STA/LTA method. However, the above models based on CNN still have the
104 problems of long training time and low computational efficiency.

Zhao Ming demonstrated that application of the U-net based model to seismic phase autoidentification has greatly improved the training speed (Zhao Ming et al. 2019), the accuracy of seismic phase identification, and the efficiency of dealing with the continuous waveform, all in comparison with STA/LTA. However, the U-net based training model still results in a 50% missed detection rate. The U-net is known for its efficient learning ability on two- or three-dimensional data. However, its high missed detection rate leads to poor learning ability for one-dimensional time series data (e.g., seismic data). In contrast, the use of Bidirectional Long Short-Term Memory (Bi-LSTM) in deep learning has proven to be efficient at processing the context of sequences and is more suitable for one-dimensional time series data. The application of Bi-LSTM to the identification and classification of heart sound signals of congenital heart disease by Zhu Lili and the pattern identification of quality control graphs by Wu Changliang have proved its efficiency with such data (Zhu Lili. 2019; Wu et al. (2019)).

To address the limitations in the application of U-net models to seismic phase autoidentification, we propose in this paper a novel U-net Bidirectional Long-Term Memory Deep Network (UBDN). This combines the advantages of U-net (e.g., fast training and accurate seismic phase identification) and Bi-LSTM (e.g., efficiency with one-dimensional time series data). The UBDN specifically maintains the accuracy of seismic phase identification. Based on that, a timing relationship can be established between seismic phase features. Seismic phase autodetection can therefore be achieved with high phase identification rates, low missed detection rates, and faster run times.

2 Methods

Taking the U-net as the framework, the structure of the UBDN model is shown in Fig.1. It can be seen that the input of the UBDN model is the original seismic waveform, and the output is marked with the P and S wave phases for the input. The blue dashed box contains the U-net component, and the red dashed box the Bi-LSTM network part. The UBDN model uses the U-net to extract and learn the P and S wave phase characteristics in the seismic waveform data, and then utilizes Bi-LSTM to identify the P and S wave phases in the new seismic waveform.

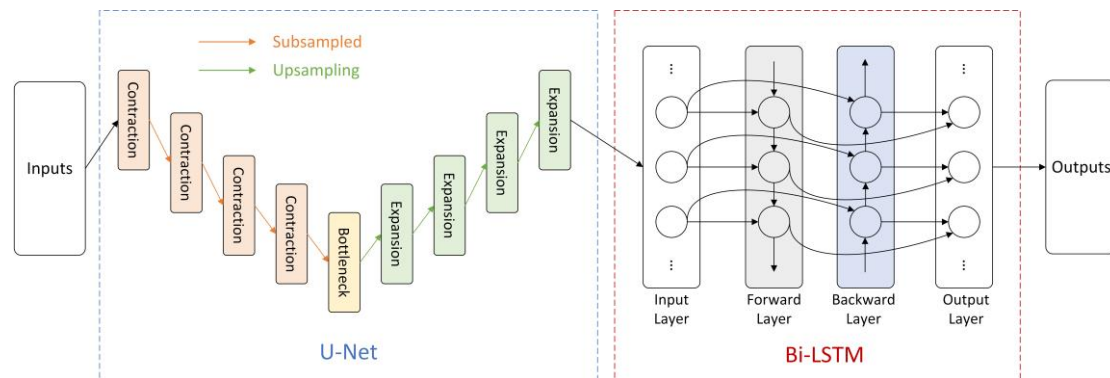


Fig.1 The UBDN model structure

The U-net realizes the extraction of the features in the seismic waveform by determining the location of the P and S phases and finding the corresponding seismic points. The U-net model structure is shown in Fig.2. The U-net consists of subsampling and upsampling layers. The subsampling layer comprises 2 one-dimensional convolutional layers and a pooling layer. In order to prevent overfitting, some dropout layers were randomly added. The upsampling layer consisted of a transposed

convolutional, cropping, and convolutional layer. A dropout layer was again randomly added to prevent overfitting. Compared with the classic U-net, the network input was processed for dimensionality reduction. The input of the U-net defaults to two- or three-dimensional image data, and the seismic waveform data were one-dimensional time series data. Therefore, all inputs and outputs inside the network needed to be reduced to one dimension. The four subsampling layers on the left side performed convolution and pooling operations to extract the abstract features of the seismic phase; whereas the four upsampling layers on the right side completed operations such as transposed convolution and connection between the left and right symmetric layers. Recovering the detailed features of the seismic phases based on the learned features on the left side was conducive to solving the problem of seismic phase classification. Finally, the probability value of P wave, S wave, or noise was calculated by the activation function, and the category of the sampling point determined by comparing with the set threshold. At the same time, a loss function was used to adjust the hyperparameters such as the weight and bias of each layer to minimize the difference between the current network's predicted value and the target value.

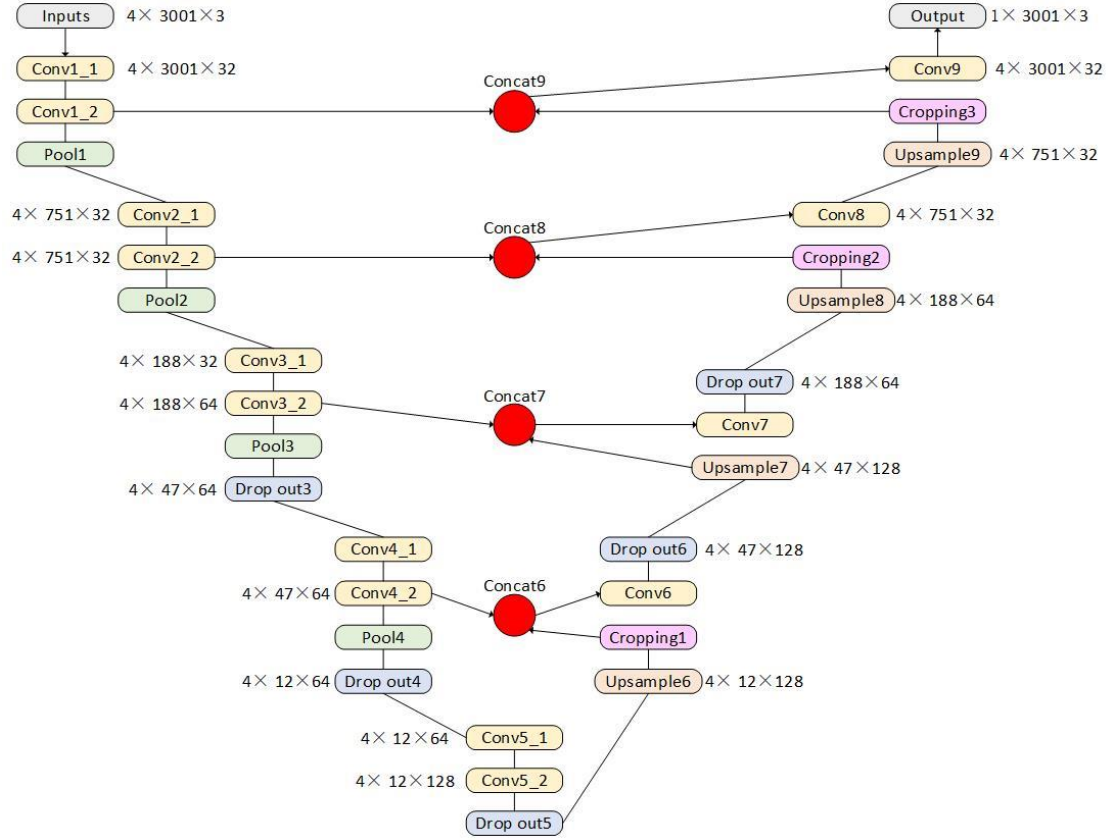


Fig.2 The U-net model structure

The loss function used in this model is shown in formula (1):

$$Loss = - \sum_{i=1}^3 \sum_{j=1}^n Y'_{ij} \cdot \log(Y_{ij}) \quad (1)$$

In formula (1), Y' is a label using binary coding; $i = 1, 2, 3$ respectively represent noise, P phase, and S phase; n is the number of waveform sampling points; and $j = 1, \dots, n$ is the sampling point number. Y' is shown in formula (2):

$$Y'_i = \begin{cases} Y'_1: [1,0,0] \\ Y'_2: [0,1,0] \\ Y'_3: [0,0,1] \end{cases} \quad (2)$$

Y is the probability value calculated by the softmax function of the last layer, as shown in formula (3):

$$Y_i = \frac{e^{z_i}}{\sum_{k=1}^3 e^{z_k}} \quad (3)$$

In formula (3), z is the output tensor ($[m, n, 3]$) of the last layer, and m is the number of input data.

The Bi-LSTM network structure is shown in Fig. 3. The network structure includes both a forward and a reverse LSTM. The forward LSTM obtains a sequence h_a according to normal input. The reverse LSTM reverses the input, and then passes it through a network with the same structure as the forward LSTM but with different weight parameters. Using this approach we eventually obtained a sequence which we then reversed to obtain h_b . Finally, we added the two sequences to get H , which is the final result through the Bi-LSTM network, as shown in formula (4).

$$H = h_a \oplus h_b \quad (4)$$

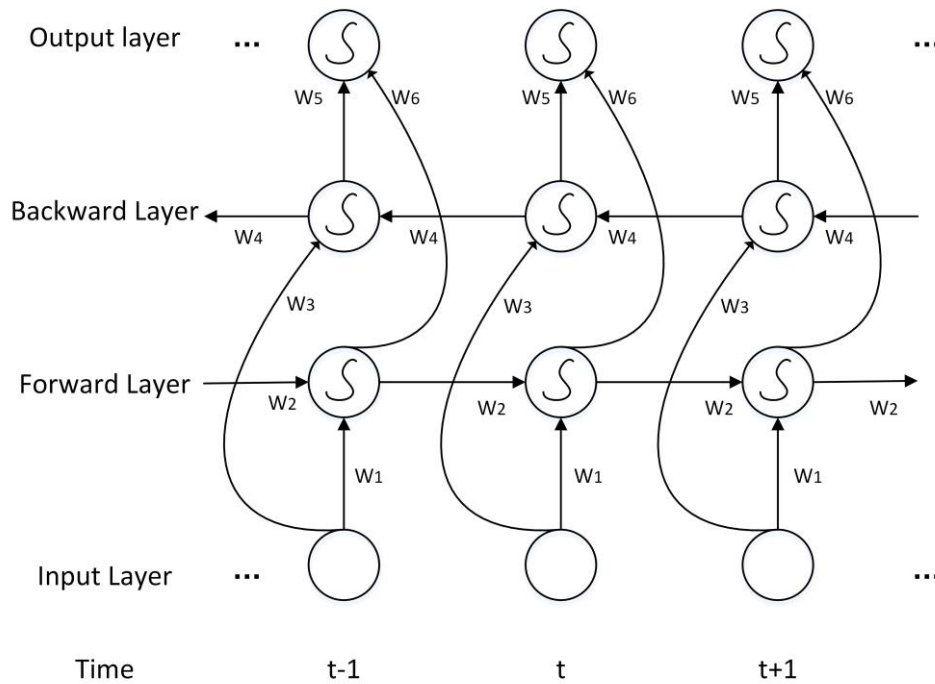


Fig. 3 The Bi-LSTM model structure

The Bi-LSTM model can simultaneously utilize historical and future information in the sequence, divide the sequence information into two directions for input into the model, use two hidden layers to store the input information in both directions, and connect the corresponding outputs of the hidden layers to the same output layer. Both of them have the same structures and are independent of each other, and they only accept different sequence inputs. Therefore, the final hidden layer contains the positive and negative time series data for the dataset. Utilizing the advantages of Bi-LSTM in processing time series data, this establishes the timing relationship between seismic phase features, which solves the problem of missed detection caused by the use of the U-net in seismic phase identification.

3 Data and evaluation indicators

3.1 Data preprocessing

The UBDN model requires a large number of preset samples for training. The sample data used here came from the Stanford Earthquake Dataset (STEAD), which is sourced mainly from the International Seismological Center, the National Earthquake Information Center, the Northern California Seismic Network, the Southern California Seismic Network, the Pacific Northwest Seismic Network, The New Madrid Seismic Network, the Incorporated Research Institutions for Seismology, the Advanced National Seismic System Composite Catalog, and the Global Seismograph Network. The STEAD comprises data recorded by seismic stations around the world from January 1984 to August 2018 (Mousavi et al. 2019). This article mainly selected seismic

204 events of a magnitude between M0.5 and 2.5 with a SNR between 20 and 30 dB; the
205 sampling rate was 100 Hz for sample data.

206 The sample data were preprocessed and the waveforms from 3s before the arrival
207 of the P wave to 10s after the arrival of the S wave selected. We then uniformly cut the
208 sample data to a length of 30s (assigned a zero value if the length is insufficient), then
209 normalized all the data as shown in formula (5), where v_i represents the amplitude
210 value of the seismic event signal, and data enhancement operations such as translation,
211 noise addition, and filtering are adopted (Hayakawa et al.1995; Schroff et al. 2015).

$$212 \quad v_i = \frac{v_i}{\max|v_i|} \quad (5)$$

213 To ensure the quality of the dataset, it was manually cleaned and obvious labeling
214 errors corrected. The final sample dataset consisted of 43,700 items, of which 80% were
215 used as training data and 20% as testing data.

216 3.2 Evaluation index

217 In order to objectively evaluate the performance of the UBDN model in practical
218 applications and ensure the reliability of the experimental results, we used the
219 calculation of the root mean square error (RMSE), accuracy (A), and missed detection
220 rate (M) of the different methods. The three formulas used to calculate these indicators
221 were as follows:

$$222 \quad RMSE = \sqrt{\frac{1}{n} \sum_{i=1}^n [(T_i - t_i)^2]} \quad (6)$$

$$223 \quad A = \frac{T_e}{(T_e + F_e)} \quad (7)$$

$$M = \frac{F_n}{(T_e + F_n)} \quad (8)$$

RMSE denotes the root mean square error between the calculated time T_i of the model and the reference mark time t_i . This was used to reflect the accuracy of the pickup time of the model. n is the number of seismic events in the dataset; i is the serial number; A represents accuracy; T_e is the number of correct detections; and F_e the number of incorrect detections. The threshold for determining correctness was set as $P \pm 0.5s$, $S \pm 0.5s$ and automatically picked up. The accuracy (A) of phase detection is the ratio of the number of phases for which the phase type is correct and within the error range identified by the model to the total number of phases. M represents the missed detection rate and F_n the number of missed seismic phases. M is computed as the ratio of the number of correct identifications to the number of manual identifications and used to check whether the model-identified seismic phase is complete relative to the reference phase, thus indicating the effectiveness of the model.

4 Experiments

Based on the UBDN model in Fig. 1, the experimental process framework design is shown in Fig. 4. It comprised three main steps: ① Data preprocessing, where the original data were cut to a uniform length, and normalization and other pretreatment procedures carried out. At the same time, data enhancement operations such as translation, noise addition, and filtering were used to enhance the generalization ability of the model, and the preprocessed dataset divided into the training and testing datasets according to the 80:20 ratio given above. ② Model training, where the relevant dataset

245 was used to train the UBDN model, the U-net to learn the seismic phase features, and
 246 the Bi-LSTM then used the features to complete the phase identification of the time
 247 series signal and output the seismic waveform data of the marked phase. ③ Model
 248 evaluation and comparison, in which we used the output model to compare the pickup
 249 and reference times, and calculated the RMSE, accuracy (A) and missed detection rate
 250 (M) to evaluate the effectiveness of the model's seismic phase identification.

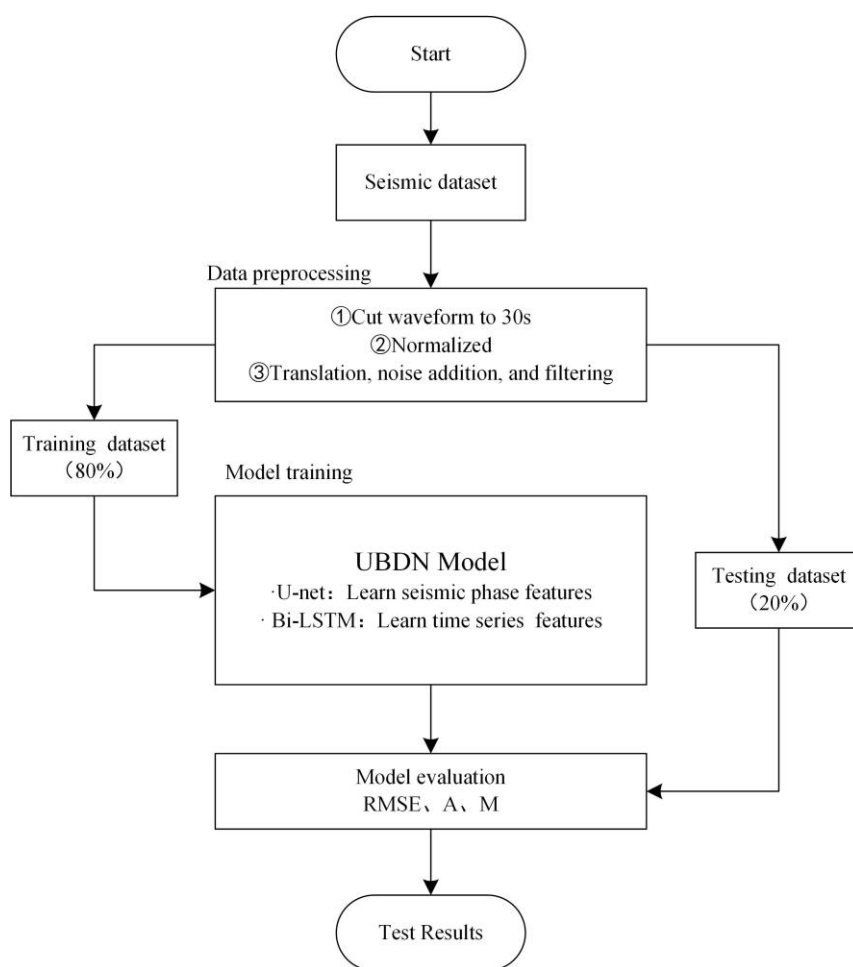


Fig. 4 Experimental flowchart

4.1 UBDN model training and testing

Firstly, the UBDN model was built and trained by Tensorflow and Keras before 80% (34,960 pieces) of waveform were selected as the training data, and 20% (8,740 pieces) as the testing dataset. The single training batch size was set to 32, the number of single training batches (n-input) to 100, and the number of earthquake events processed by a single training (n-step) set to 100. The UBDN model training used cross-entropy as the loss function and adopted the Adam algorithm to optimize the loss function calculation process. The Adam algorithm can speed up the convergence speed of the model because it has the advantages of high computational efficiency and adaptive learning rate. L2 regularization was used to prevent overfitting (Kingma et al. 2014).

Fig. 5 shows the training and testing results of the UBDN model. Fig. 5(a) denotes the training accuracy of the model; Fig. 5(b) its loss function value; Fig. 5(c) the phase identification accuracy (A) of the P wave on the testing dataset; and Fig. 5(d) the phase identification accuracy (A) of the S wave on the testing dataset. It can be seen from Fig.s 5(a) and 5(b) that the UBDN model had an accuracy (A) of 98% after training the fourth cycle (about 20,000 time steps), and the loss value dropped to 0.03. The accuracy (A) and loss values of the following five cycles remained at this level, which shows that the UBDN model converged at this point after about 45,000 time steps. Fig.s 5(c) and 5(d) show that the accuracy (A) of the P and S wave phase identification on the testing dataset increased over time. From time steps 10,000 to 45,000, the P and S waves increased from 65.1% and 43.7% to 90.1% and 89.5% respectively. This indicates that

275 the model did not overfit; furthermore, the longer the training time, the higher the
 276 accuracy. The experimental results in Fig. 5 show that the accuracy (A) of phase
 277 identification of P and S waves by the model was 90.1% and 89.5%, respectively, which
 278 meets the accuracy requirements for seismic phase identification. This indicates the
 279 model can be used effectively for this purpose.

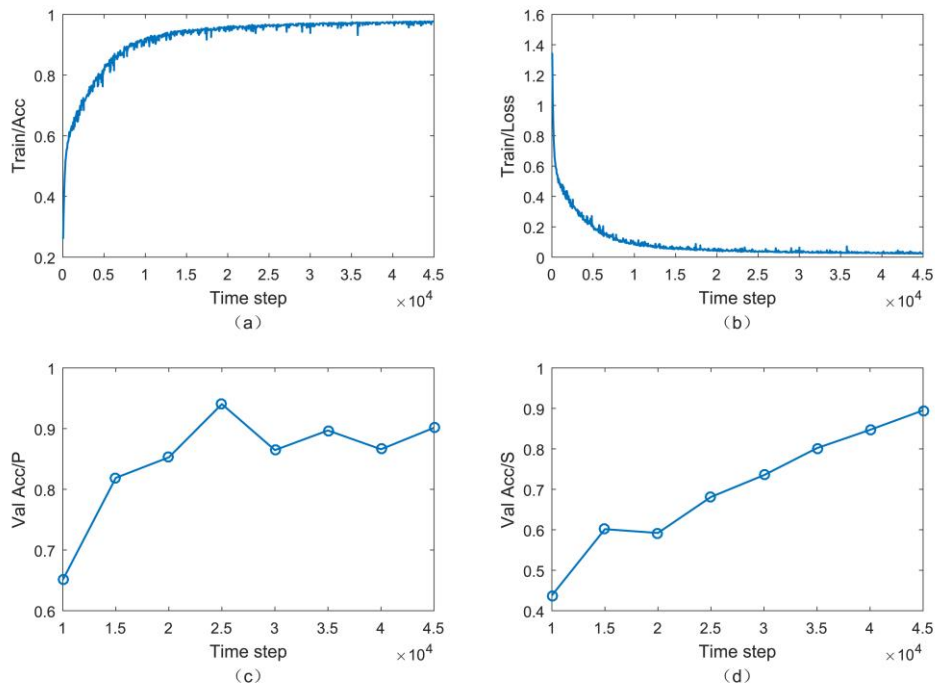


Fig. 5 Training and testing process of the UBDN model

4.2 Comparative Experiments

In order to verify the seismic phase identification ability of the UBDN model, we compared it with the deep learning U-net [19], STA/LTA, and AIC seismic phase identification methods. In the comparative experiments, all models used a unified dataset of 2,000 pieces of waveform, and the SNR was concentrated between 20~30dB. We used formulas (6), (7), and (8) to calculate the RMSE, accuracy (A), and missed

detection rate (M) so as to evaluate the detection results of the four models. The experimental results are shown in Table 1.

Table 1 – Comparison of the UBDN model with the U-net, STA/LTA, and AIC methods

Method		RMSE	A	M
UBDN	P	0.26	87.99%	11.45%
	S	0.27	87.60%	14.58%
U-net	P	0.35	81.26%	30.74%
	S	0.41	83.49%	28.40%
STA/LTA	P	0.49	73.45%	37.52%
	S	0.62	76.23%	35.87%
AIC	P	0.43	75.13%	32.81%
	S	0.58	78.92%	30.72%

As can be seen from Table 1, the RMSE of the UBDN model for the P and S waves was 0.26s and 0.27s, and the accuracy (A) was 87.99% and 87.61%. This represents a significant improvement over the traditional STA/LTA and AIC methods. The UBDN model also shows improvement in comparison with the U-net model. This indicates the UBDN model has obvious advantages compared with other methods in terms of accuracy. In terms of missed detection rates, the parameter M for the UBDN model was 11.45% and 14.58%. Compared with other methods, this is a significant reduction and

indicates that the combination of the U-net and Bi-LSTM network approaches has achieved an ideal result in reducing the missed detection rate. The three evaluation indicators were highest for the UBDN model among the four methods tested.

Fig. 6 shows the various possible scenarios for the UBDN model in the phase identification process. In the Fig., the black line shows when the P wave is picked up manually, and the red line when the S wave is picked up manually. Fig. 6(a) shows the correct detection of the P and S wave phases; Fig. 6(b) the correct detection of the P-wave phase and the incorrect detection of the S-wave phase; Fig. 6(c) shows the S-wave phase detected and the P-wave phase; Fig. 6(d) shows the reverse scenario.

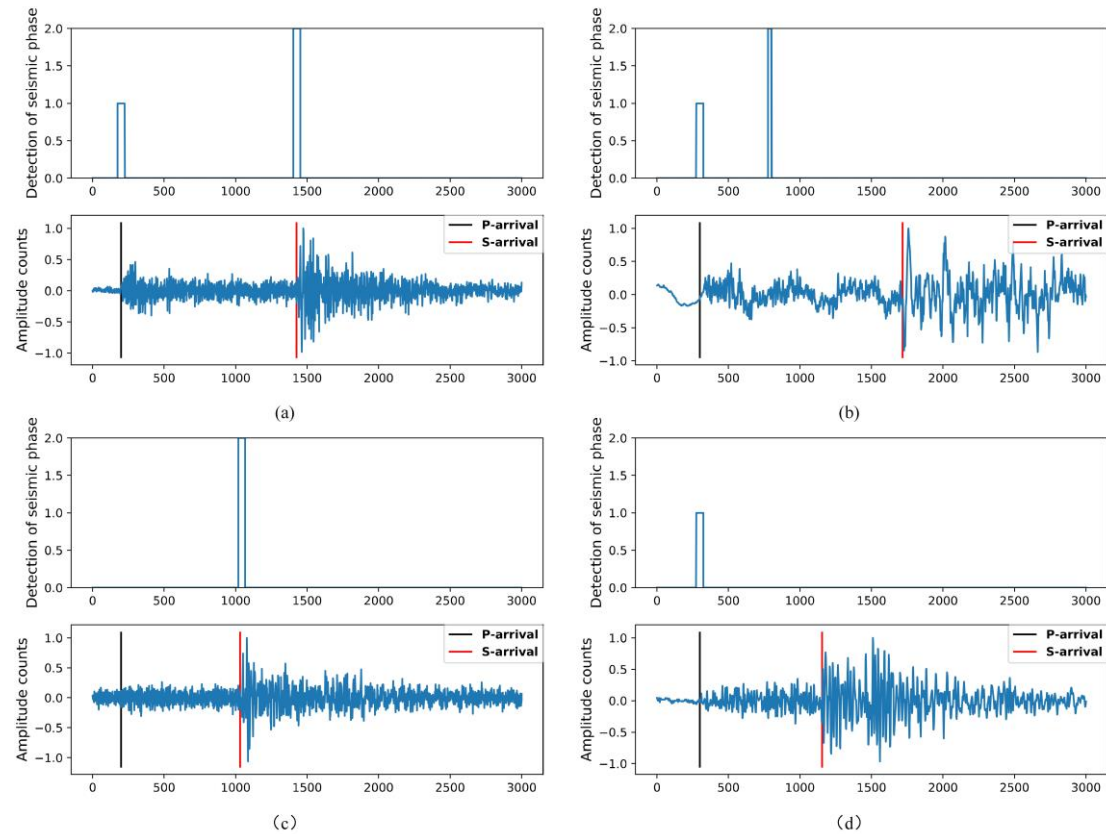


Fig. 6 Different phase identification scenarios for the UBDN model

4.3 Application of the Model to the Wenchuan Earthquake Aftershocks

In order to verify the phase identification effect of the UBDN model in an actual earthquake event, it was applied to the aftershock dataset of the Wenchuan earthquake from May to September 2008. This dataset contains both seismic events and phase data. A total of 2,026 phase data items were collected from 76 stations. The SNR of the data was concentrated between 2~5dB, the sampling rate was 200Hz, and the attribute fields included the earthquake time and longitude, latitude, depth, magnitude type, magnitude, reference location, event type, and so on (Data sharing infrastructure of national earthquake data center - <http://data.earthquake.cn>). An example event is shown in Fig. 7. This depicts the seismic events taking place at 14:53 on May 12, 2008. The magnitude is Ms6.3; the focal depth 14km as recorded by the Maoxin Nanxin station (51MXN); the black line denotes the arrival of the manually picked P wave; and the red line the arrival of the manually picked S wave. Fig.s 7(a), 7(b), and 7(c) represent the vertical, north-south, and east-west seismic waveforms, respectively. The UBDN model was used to identify the phases of the Wenchuan earthquake aftershock dataset. The results are shown in Table 2.

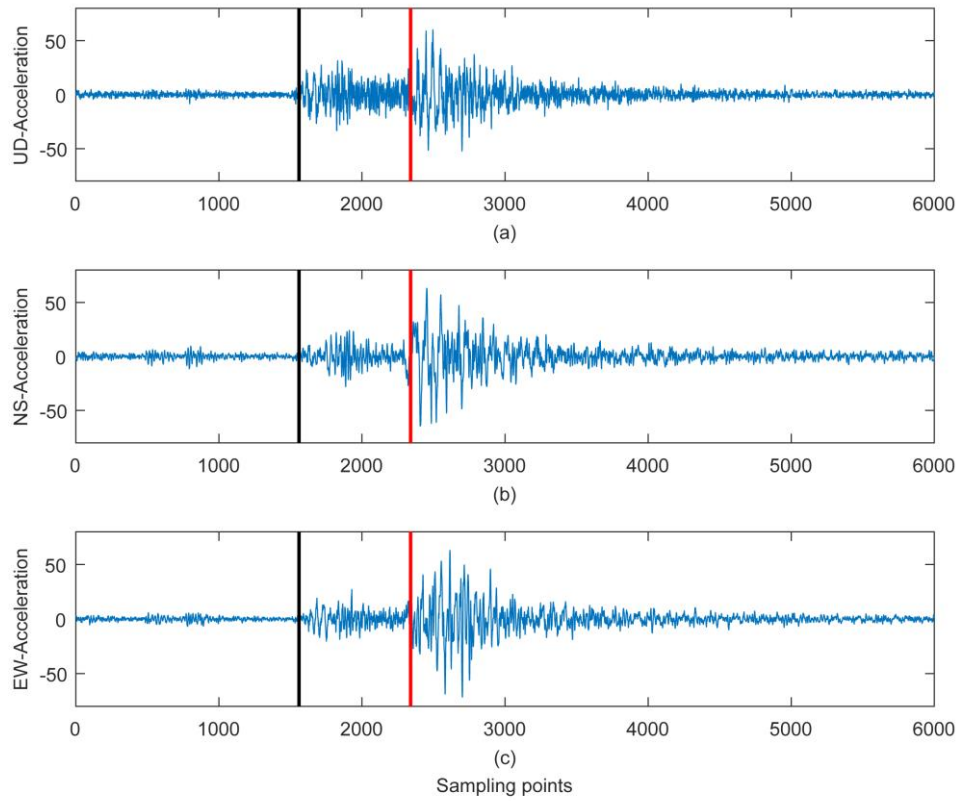


Fig. 7 Examples of seismic event waveforms

Table 2 Phase identification results for the UBDN model on the Wenchuan earthquake aftershock dataset

Method		RMSE	A	M
UBDN	P	0.31	80.69%	17.18%
	S	0.34	77.87%	20.56%

It can be seen from Table 2 that the RMSE of the UBDN model on the Wenchuan earthquake aftershock dataset was 0.31s and 0.34s, the accuracy (A) 80.69% and 77.87%, and the missed detection rate (M) 17.18% and 20.56%. Compared with the experimental results of the testing dataset, the effect of the UBDN model on the

Wenchuan earthquake aftershock dataset is slightly poorer. This may be attributable to the different SNR of the datasets. To verify this hypothesis, the SNR of the aftershock dataset was concentrated in the range 2~5dB, and the SNR of the testing dataset in the range 20~30dB. Phase identification tests were then performed on five datasets with different SNR ranges of 0~10dB, 10~20 dB, 20~30 dB, 30~40 dB, and >40 dB, with the number of events in each dataset set as 1,000.

The results of this experiment are shown in Fig. 8. It can be seen that the RMSE, accuracy (A), and missed detection rate (M) all have a linear relationship with SNR. As the SNR increases, RMSE and M gradually decrease, but A gradually rises. This indicates that the higher the SNR of the data, the better the seismic phase identification of the UBDN model. Although the effect for the actual Wenchuan earthquake aftershock dataset is slightly lower than that for the testing dataset, it can still meet the needs of practical applications. Therefore, the UBDN model has a certain degree of adaptability, and can still achieve a good seismic phase identification effect under the condition of low SNR.

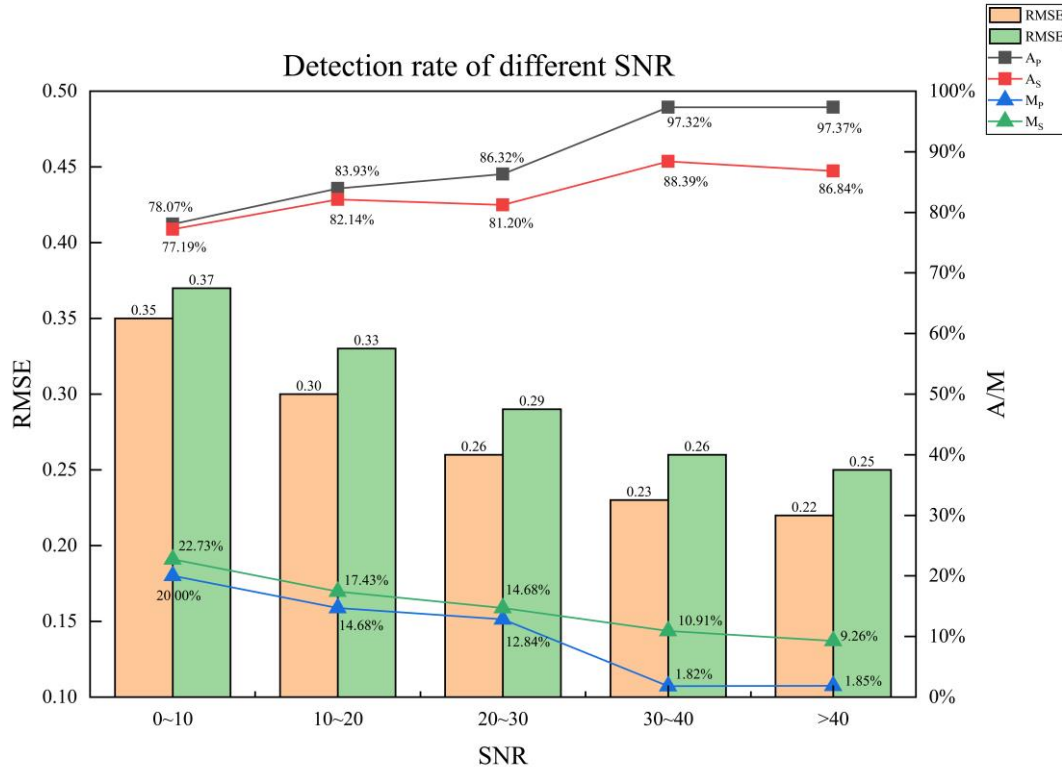


Fig. 8 Phase identification results for datasets with different SNR

5 Conclusion

Based on U-net and Bi-LSTM structures, we designed a UBDN seismic phase automatic identification model, used it to train a dataset, and established the relationship between the phase arrival time and the seismic waveform phase for real-time identification. By comparing the results of the trained model with those for other identification methods, and performing testing and experimental analysis using the 2008 Wenchuan earthquake aftershock dataset, we can draw the following conclusions. Firstly, the UBDN model can achieve sufficient accuracy to meet the requirements of seismic phase identification; secondly, compared with other methods, it offers a significant improvement on accuracy and a significant reduction in the missed detection

rate; and thirdly, using the UBDN model with a real-life dataset (i.e., the Wenchuan earthquake aftershock data) shows that there is still a strong phase identification effect and further indicates that the model has good adaptability.

In practical applications, low-SNR data have an impact on the identification capabilities of the UBDN model. Future research may consider using seismic data collected by the same type of instrument and processed by the same noise reduction method as a dataset for model training, according to the noise level and sensitivity of seismic instruments and the difference in data noise reduction methods. This approach can greatly reduce the influence of SNR on the results of the UBDN model training and identification process and thus improve its stability.

Declarations

Ethics approval and consent to participate

Not applicable.

Consent for publication

Not applicable.

Availability of data and materials

The datasets used and/or analyzed during the current study are available from the corresponding author upon reasonable request.

Competing interests

The authors declare no conflict of interests.

Funding

This work was supported by the Special Fund of Fundamental Scientific Research Business Expense for Higher School of Central Government [no. ZY20180111], The National Key Research and Development Programme of China (Grant No 2018YFC1503801), and the Scientific Research Project Item of Hebei Province Education Department (Grant No.QN2018317).

Authors' contributions

Jianxian Cai, Zhitao Gao contributed to the conception of the study; Jianxian Cai, Xun Dai performed the experiment; Xun Dai, Zhitao Gao contributed significantly to analysis and manuscript preparation; Jianxian Cai, Xun Dai performed the data analyses and wrote the manuscript; Jianxian Cai, Zhitao Gao, Yan Shi helped perform the analysis with constructive discussions.

Acknowledgements

Acknowledgement for the data support from " China Earthquake Networks Center, National Earthquake Data Center. (<http://data.earthquake.cn>)"; Acknowledgement for the data support from " the Stanford Earthquake Dataset (STEAD). (<https://github.com/smousavi05/STEAD>)".

399 **References**

- 400 Akaike H (1974) A new look at the statistical model identification. IEEE Transactions
401 on Automatic Control 19(6): 716-723.
- 402 Akazawa T (2004) A technique for automatic detection of onset time of P-and S-phases
403 in strong motion records.In:The 13th World Conference on Earthquake Engineering:
404 International Association of Earthquake Engineering, Vancouver BC, Canada, January
405 2004.
- 406 Allen R V (1978) Automatic earthquake recognition and timing from single traces.
407 Bulletin of the Seismological Society of America 68(5): 1521-1532.
- 408 Baer M, Kradolfer U (1987) An automatic phase picker for local and teleseismic events.
409 Bulletin of the Seismological Society of America 77(4): 1437-1445.
- 410 Boschetti F, Dentith M D, List R D, (1996) A fractal-based algorithm for detecting first
411 arrivals on seismic trances. Geophysics 61(4): 1095-1102.
412 <https://doi.org/10.1190/1.1444030>
- 413 Cao Maosen, Ren Qingwen, Wan Linmei, Luo Yong (2004) Length Picking up first
414 arrival of seismic wave with fractal dimension algorithm.Petroleum geophysical
415 exploration (05): 510-514.
- 416 Chang Xu, Liu Yike (2002) Generalized fractal dimension of seismic records and its
417 application.Acta geophysica Sinica (06): 839-846. doi:10.3321/j.issn:0001-
418 5733.2002.06.011

419 Dai H, MacBeth C (1997) The application of back-propagation neural network to
 420 automatic picking seismic arrival from single-component recordings. Journal of
 421 Geophysical Research: Solid Earth (1978-2012) 102(B7): 15105-15113.

422 Han Xiaojun, Shi zejin, Li Yalin (2002) An improved algorithm for picking up the first
 423 arrival of seismic wave using fractal dimension. Petroleum geophysical exploration
 424 37(1): 60-63. doi:10.3321/j.issn:1000-7210.2002.01.012

425 Hayakawa, Marumoto, Sawada (1995) Effects of the chaotic noise on the performance
 426 of a neural network model for optimization problems. Physical review. E, Statistical
 427 physics, plasmas, fluids, and related interdisciplinary topics 51(4): R2693-R2696.
 428 <https://doi.org/10.1103/PhysRevE.51.R2693>

429 Kingma D. P, Ba J, Adam (2014). A method for stochastic optimization. arXiv preprint
 430 arXiv:1412.6980.

431 Liu Jinsong, Wang Yun, Yao Zhenxing (2013) Automatic picking up method of
 432 microseismic signals when they arrive. Acta geophysica Sinica 56(5): 1660-1666,
 433 doi:10.6038/cjg20130523. doi:10.6038/cjg20130523

434 Mousavi S M, Sheng Y, Zhu W, et al. (2019). Stanford Earthquake Dataset (STEAD):
 435 A global dataset of seismic signals for AI. IEEE Access: 179464-179476. doi:
 436 10.1109/ACCESS.2019.2947848

437 Perol T, Gharbi M, Denolle M A (2018) Convolutional neural network for earthquake
 438 detection and location. Science Advances 4(2). doi: 10.1126/sciadv.1700578

439 Ross Z E, Meier M A, Hauksson E (2018) P wave arrival picking and first-motion
 440 polarity determination with deep learning. *Journal of Geophysical Research: Solid*
 441 *Earth* 123(6): 5120-5129. <https://doi.org/10.1029/2017JB015251>
 442 Ross Z E, Meier M A, Hauksson E, Heaton T H (2018) Generalized seismic phase
 443 detection with deep learning. *Bulletin of the Seismological Society of America* 108(5A):
 444 2894-2901. <https://doi.org/10.1785/0120180080>
 445 Schroff F, Kalenichenko D, Philbin J (2015) FaceNet: A unified embedding for face
 446 recognition and clustering. 2015 IEEE Conference on Computer Vision and Pattern
 447 Recognition (CVPR). Boston, MA, USA: IEEE: 815-823.
 448 Sleeman R, Van Eck T (1998) Robust automatic P-phase picking: an on-line
 449 implementation in the analysis of broadband seismogram recordings. *Physics of the*
 450 *Earth and Planetary Interiors* 113(1-4): 265-275. [https://doi.org/10.1016/S0031-](https://doi.org/10.1016/S0031-9201(99)00007-2)
 451 [9201\(99\)00007-2](https://doi.org/10.1016/S0031-9201(99)00007-2)
 452 Tang Yalei (2017) Application of fractal theory in P-wave phase identification.
 453 Dissertation, Southwest Jiaotong University.
 454 Wang Ji, Chen Jiuhui (2008) Automatic detection of seismic events using artificial
 455 neural network. *Seismogeomagnetic observation and research* (03): 41-45.
 456 [doi:10.3969/j.issn.1003-3246.2008.03.007](https://doi.org/10.3969/j.issn.1003-3246.2008.03.007)

457 Wang Jinfeng, Luo Shengxian (2006) BP improvement of neural network and its
 458 application in first break picking. Calculation technology of geophysical and
 459 geochemical exploration (01): 14-17. doi:10.3969/j.issn.1001-1749.2006.01.005

460 Withers M, Aster R, Young C, Beiriger J, Harris M, Moore S, Trujillo J (1998) A
 461 comparison of select trigger algorithms for automated global seismic phase and event
 462 detection. Bulletin of the Seismological Society of America 88(1): 95-106.

463 Wu Changliang, Zhu Bo, Wan Yuwei, Zhao Shengran (2019) Pattern recognition of
 464 quality control chart based on Bi LSTM. Software 40(07): 89-95.
 465 doi:10.3969/j.issn.1003-6970.2019.07.016

466 Wu Dongpo (2004) Research on real time method of seismic phase identification.
 467 Dissertation, Institute of engineering mechanics, China Seismological Bureau.

468 Yu Ziyue, Chu Risheng, Sheng Minhan (2018) Deep neural network picking up P and s
 469 arrival time of earthquake. Acta geophysica Sinica 61(12): 4873-4886.
 470 doi:10.6038/cjg2018L0725

471 Zhang Fanmin, Li Qinghe, Zhang Yuansheng, Sheng Guoying, Fan Bing (1998) Using
 472 artificial neural network theory to identify seismic signal and seismic phase[J]. Journal
 473 of Northwest seismology (04): 43-49.

474 Zhao Ming, Chen Shi, Fang Lihua, Yuen D A (2019) Study on the method of seismic
 475 phase identification and arrival time picking based on U-shaped convolution neural
 476 network. Acta geophysica Sinica 62(08): 3034-3042. doi:10.6038/cjg2019M0495

477 Zhao Ming,Chen Shi,Yuen D (2019) Automatic classification and recognition of
478 seismic waveform based on deep learning convolutional neural network.Acta
479 geophysica Sinica 62(1): 374-382. doi:10.6038/cjg2019M0151.

480 Zhu Lili (2019) Recognition of congenital heart disease based on Bi LSTM network.
481 Dissertation,Yunnan University.

482

483

Figures

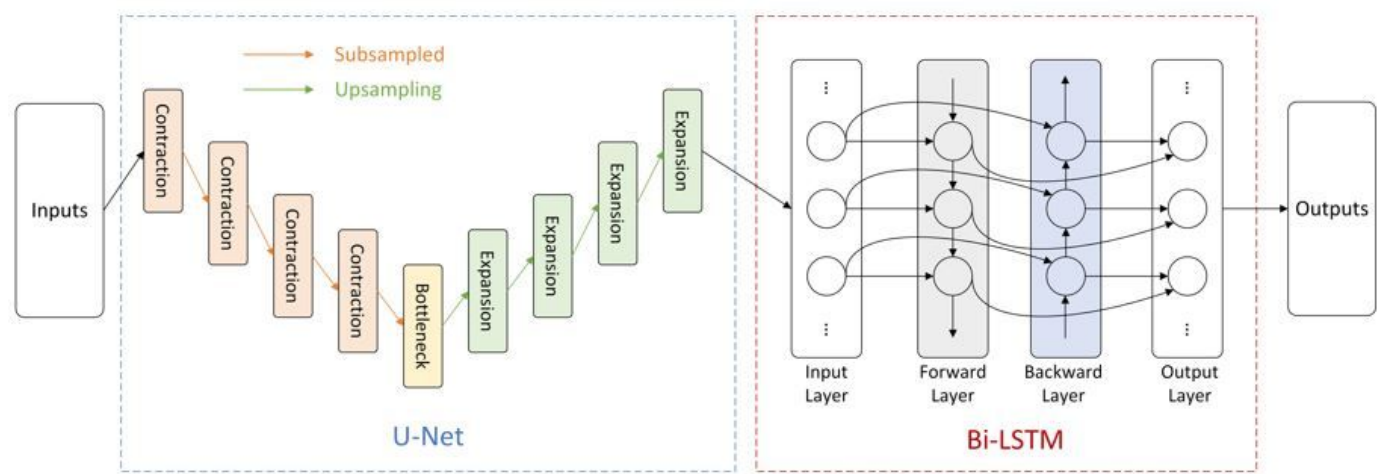


Figure 1

The UBDN model structure

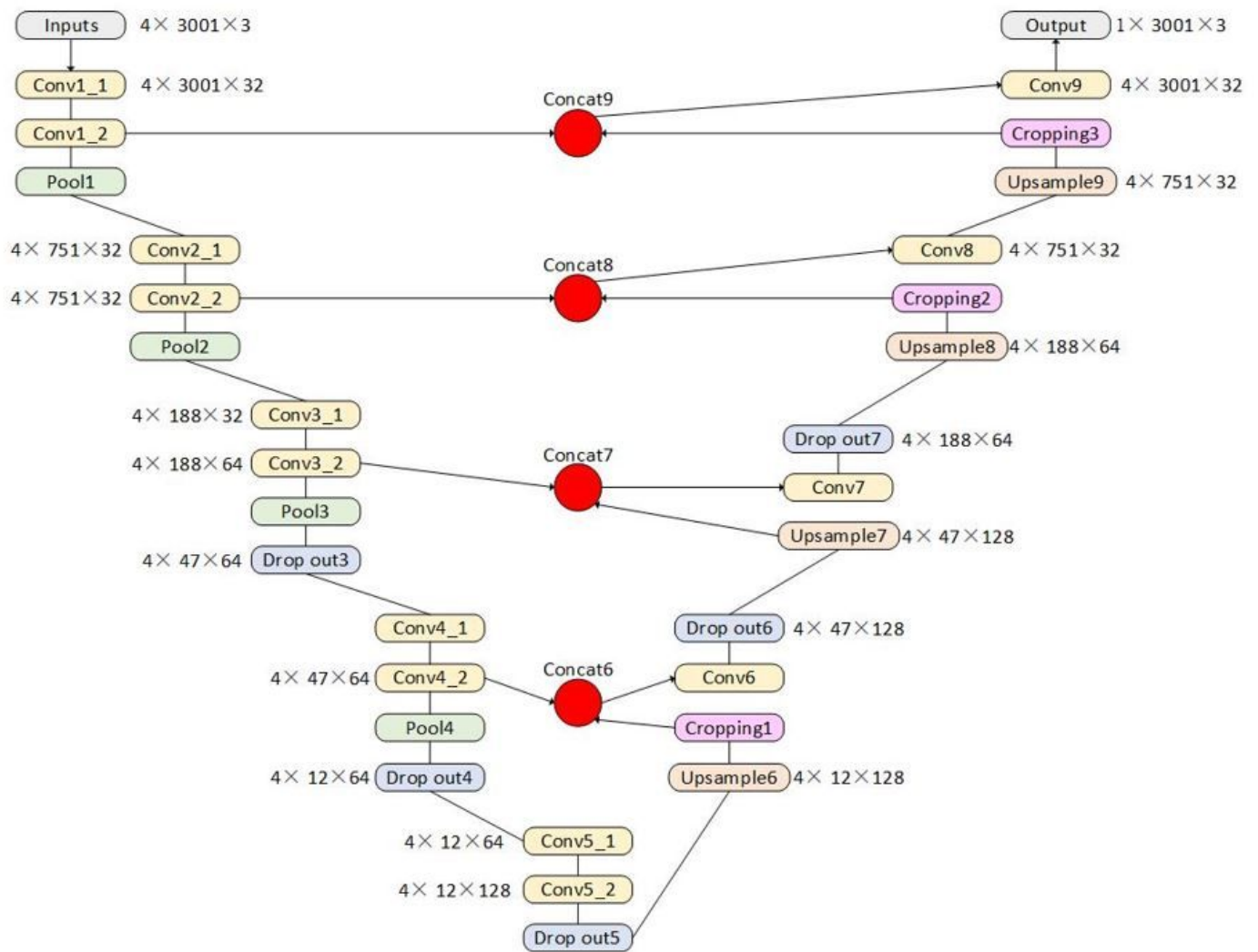


Figure 2

The U-net model structure

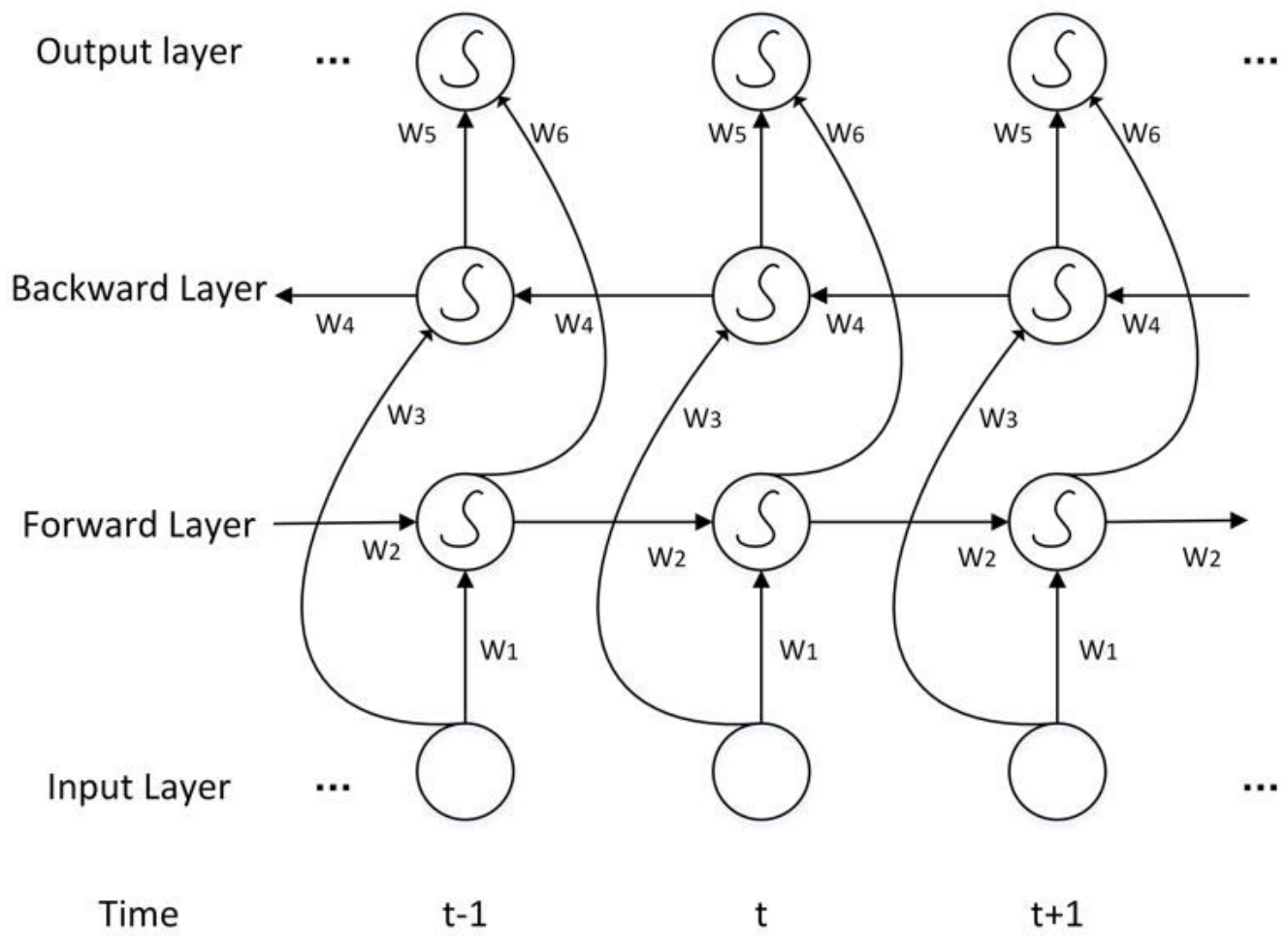


Figure 3

The Bi-LSTM model structure

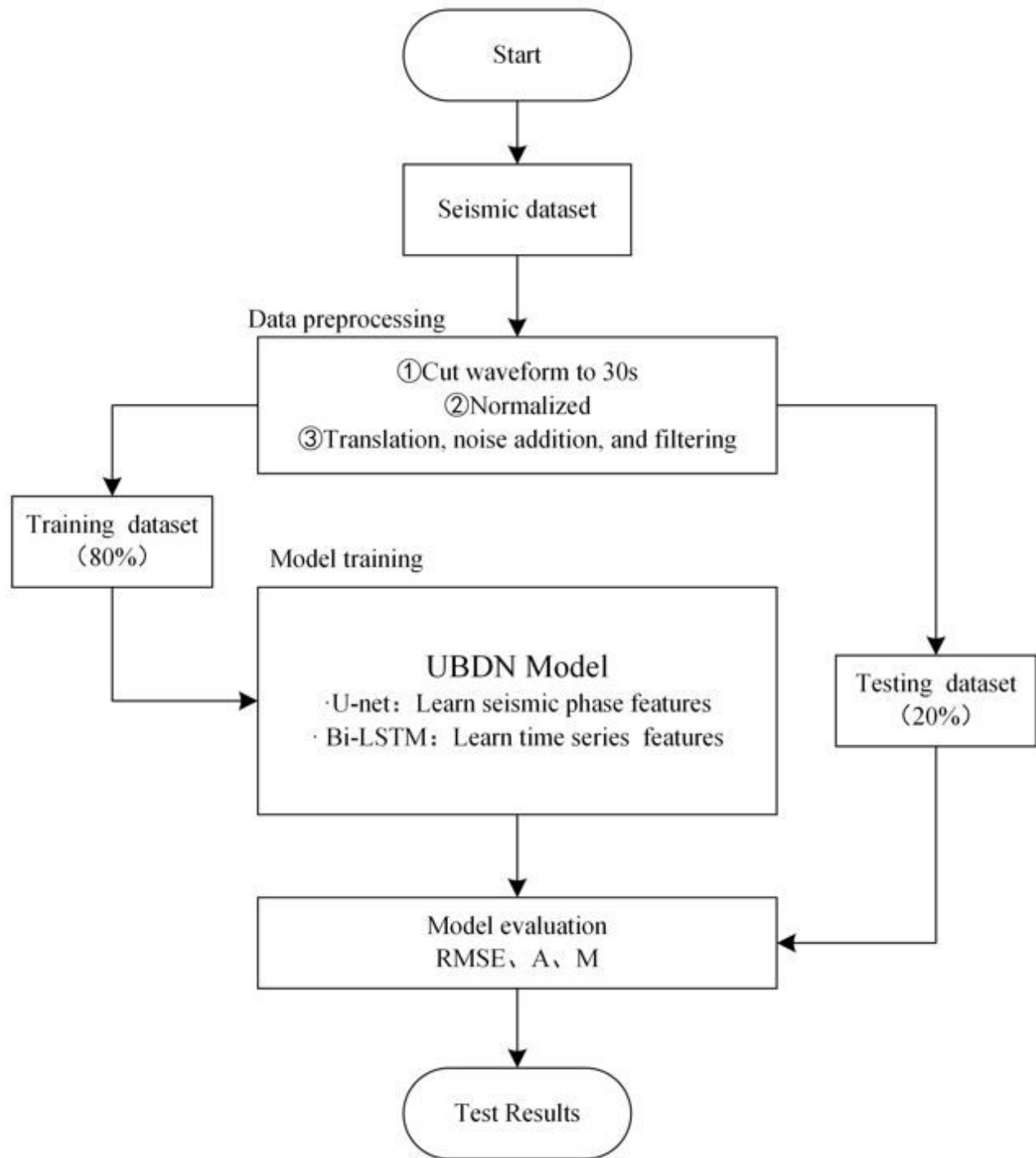


Figure 4

Experimental flowchart

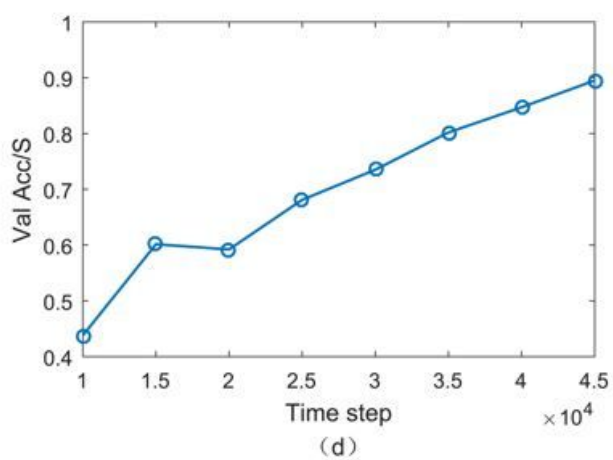
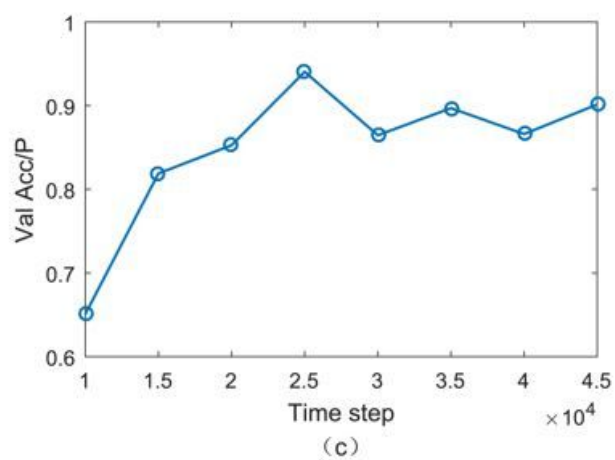
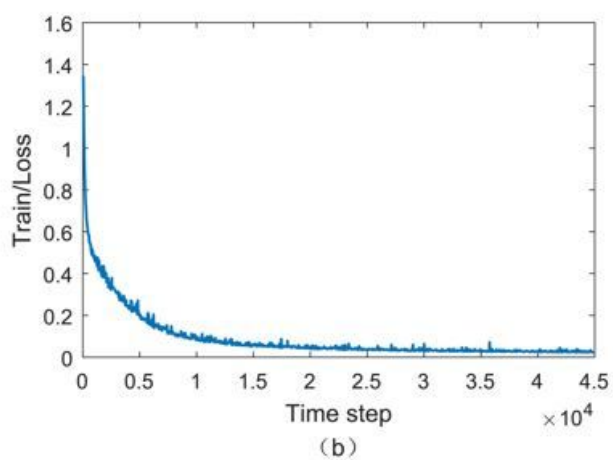
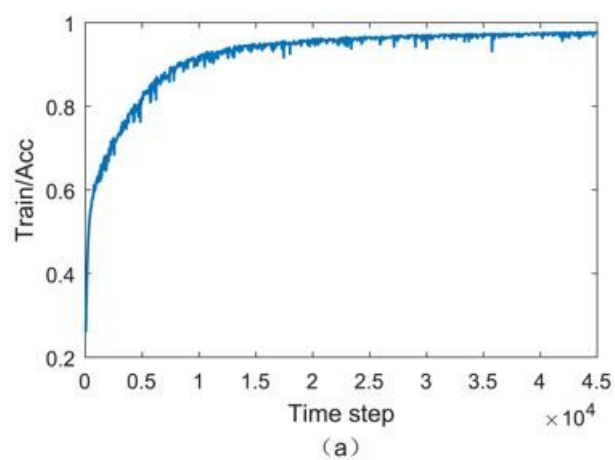


Figure 5

Training and testing process of the UBDN model

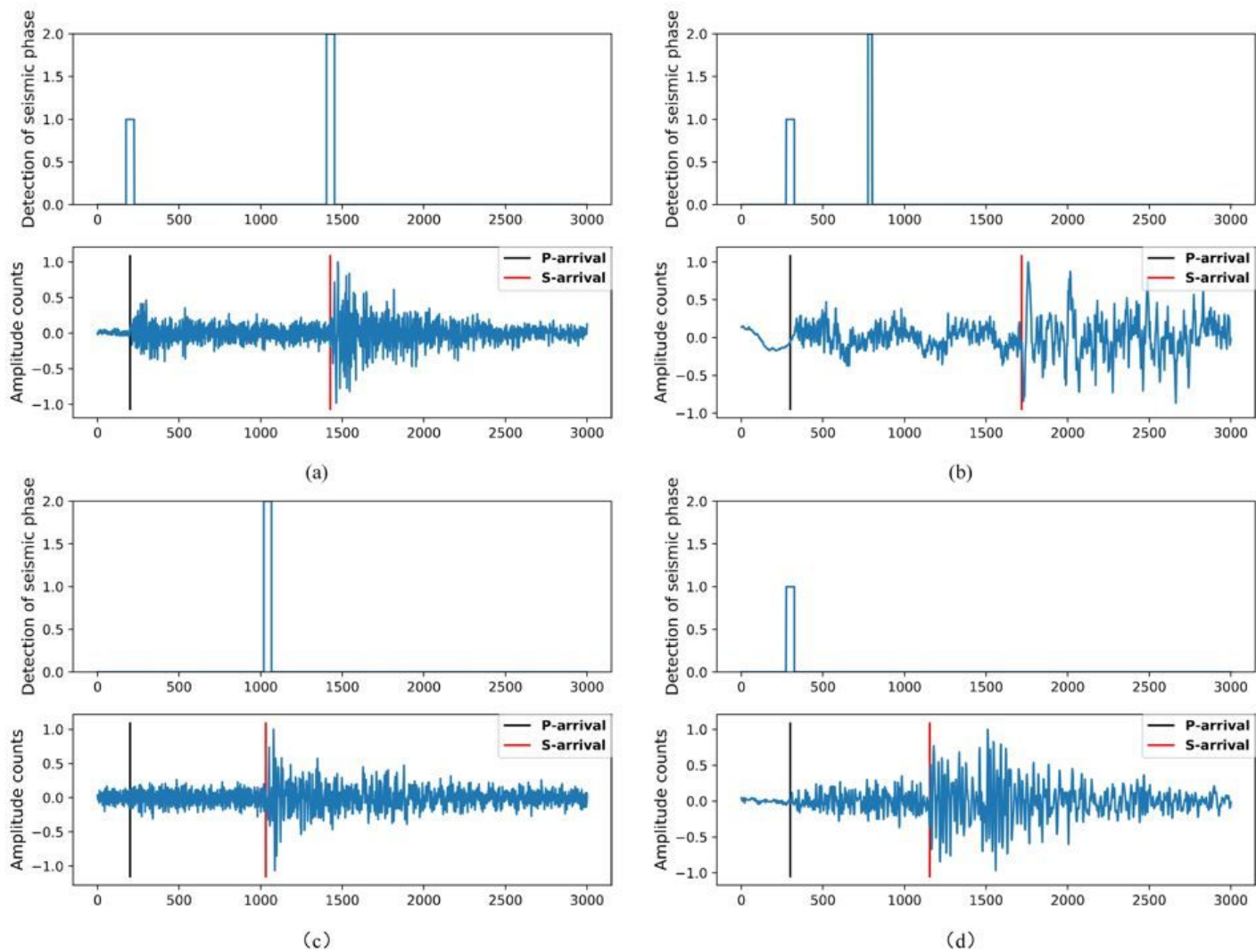


Figure 6

Different phase identification scenarios for the UBDN model

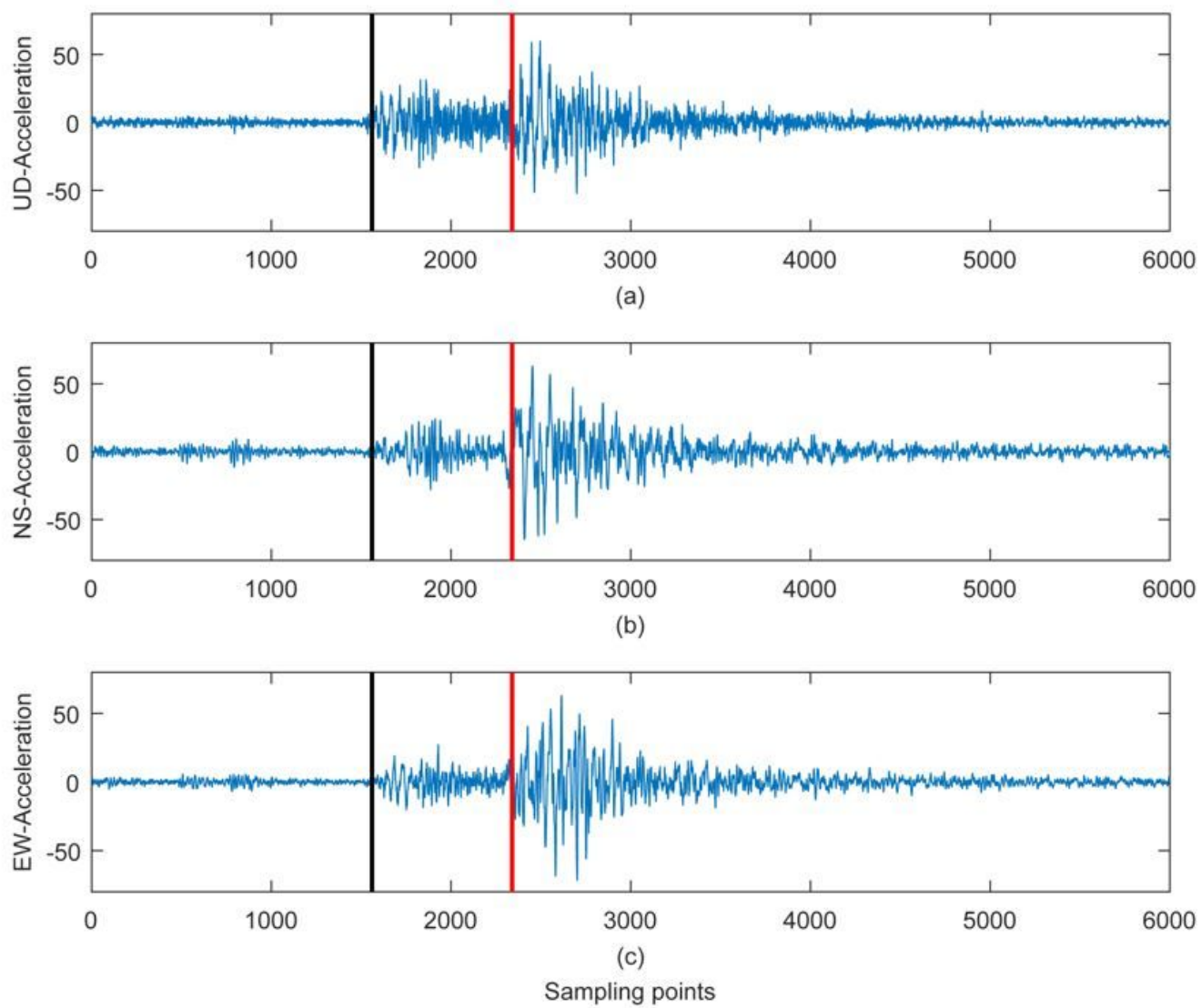


Figure 7

Examples of seismic event waveforms

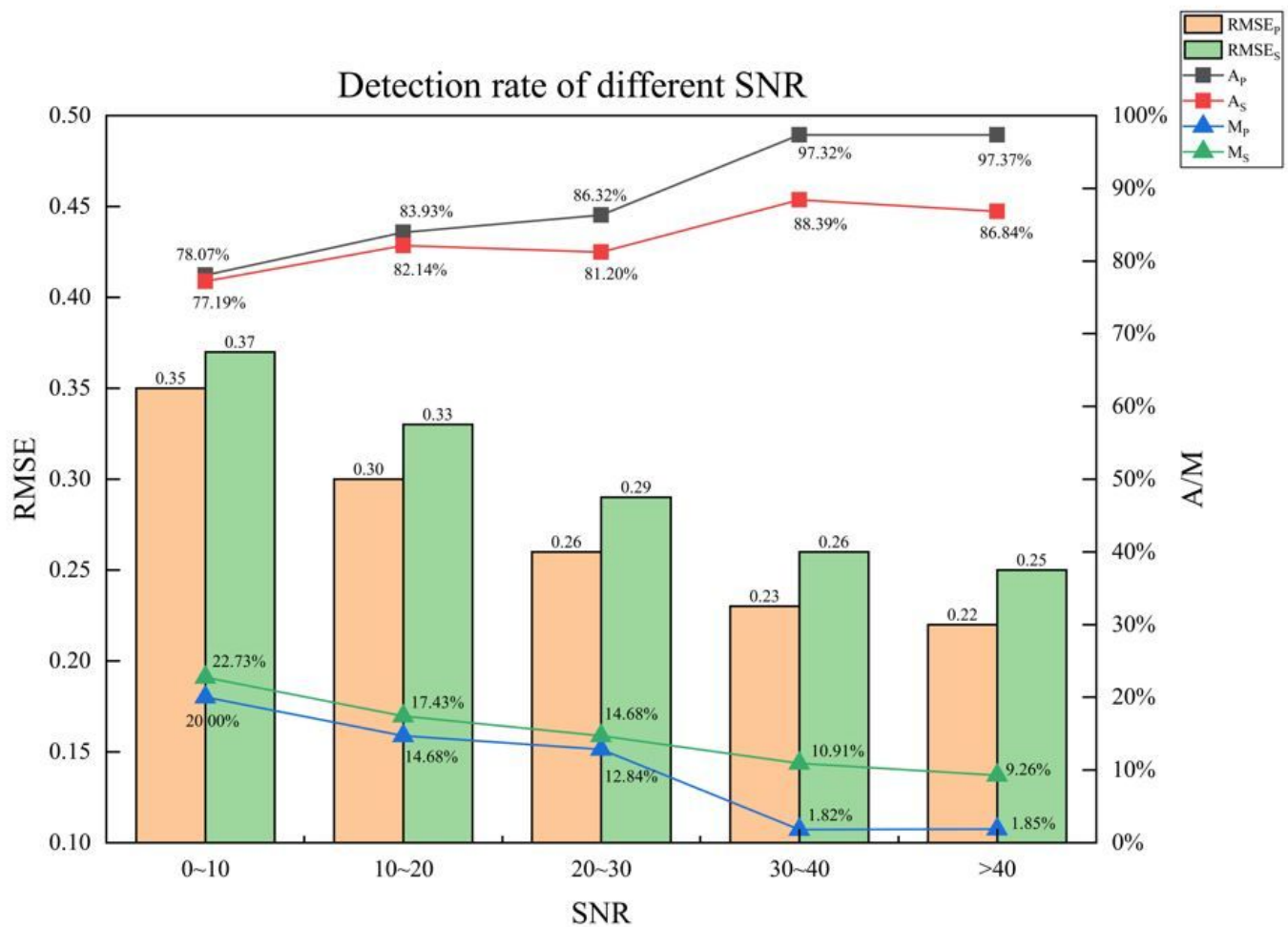


Figure 8

Phase identification results for datasets with different SNR

Supplementary Files

This is a list of supplementary files associated with this preprint. Click to download.

- [Graphicalabstract.png](#)